Journal of Solid State Chemistry 183 (2010) 1159–1164

Contents lists available at ScienceDirect

Journal of Solid State Chemistry

journal homepage: www.elsevier.com/locate/jssc

Lanthanide oxalatophosphonates with two- and three-dimensional structures

Ting-Hai Yang [a,b], Deng-Ke Cao [a], Yi-Zhi Li [a], Li-Min Zheng [a,*]

[a] State Key Laboratory of Coordination Chemistry, Coordination Chemistry Institute, Nanjing University, Nanjing 210093, PR China
[b] High-Tech Research Institute of Nanjing University, Changzhou 213164, Jiangsu, PR China

ARTICLE INFO

Article history:
Received 15 September 2009
Received in revised form
26 February 2010
Accepted 8 March 2010
Available online 12 March 2010

Keywords:
2-pyridylmethylphosphonic acid
Lanthanide oxalatophosphonate
Crystal structure
Luminescence
Magnetic property

ABSTRACT

Reactions of lanthanide nitrate, oxalate sodium and 2-pyridylmethylphosphonic acid (2-pmpH$_2$) under hydrothermal conditions result in five new lanthanide oxalatophosphonates with two types of structures. Compounds [Ln_4(ox)$_5$(2-pmpH)$_2$(H$_2$O)$_7$]·5H$_2$O [Ln^{3+}=Gd (**1**), Tb (**2**), Dy (**3**); ox^{2-}=C$_2$O$_4^{2-}$] exhibit a double layer structure, made up of net-like {Ln_4(ox)$_5$}$_n$ layers containing Ln_{10}(ox)$_{10}$ rings which are connected by 2-pmpH$^-$. While compounds [Ln_4(ox)$_5$(2-pmpH)$_2$(H$_2$O)$_6$]·6H$_2$O [Ln^{3+}=Ho (**4**), Yb (**5**)] display a three-dimensional framework structure in which the {Ln_4(ox)$_5$}$_n$ layers are cross-linked by 2-pmpH. The solid state luminescent and magnetic properties are investigated.

1. Introduction

Metal phosphonate compounds have gained increasing attention owing to their potential application in exchange and sorption [1–4], catalysis [5–7], magnetism [8–11] and optics [12,13]. Lanthanide-based compounds can exhibit excellent photophysical properties, contributing to *f*–*f* transitions with an extremely narrow bandwidth [14–17]. A number of lanthanide phosphonates have been reported so far, most of which were synthesized by employing phosphonate ligands containing functional groups in order to improve the solubility and hence the crystallization of the products [18]. Another approach that has been much less explored is to introduce a second ligand such as oxalate (ox^{2-}) into the reaction system. It is well known that oxalate is able to mediate electronic effects between paramagnetic metal ions. It can also act as a linker between metal centers to yield structures ranging from zero-dimensional species to three-dimensional open framework [19,20]. However, very few lanthanide oxalatophosphonates have been reported so far, including [*Ln*(ox){MeNH(CH$_2$CO$_2$)(CH$_2$PO$_3$H)}]·0.5H$_2$O (*Ln*=Nd, Eu, Gd), [Ln_4(ox)$_5$(Me$_2$NHCH$_2$PO$_3$)$_2$(H$_2$O)$_4$]·2H$_2$O (*Ln*=La, Nd), [Ln_3(ox)$_4$(Me$_2$NHCH$_2$PO$_3$)(H$_2$O)$_6$]·6H$_2$O (*Ln*=Gd, Er) [21], [La$_2$(ox)$_2$(H$_6$L)]·2H$_2$O and Ln_2(ox)$_2$(H$_6$L)(H$_2$O)$_2$·4H$_2$O [*Ln*=Nd, Eu; H$_8$L=(H$_2$O$_3$PCH$_2$)$_2$N(CH$_2$)$_4$N(CH$_2$PO$_3$H$_2$)$_2$] [22], Na[Ln_3(H$_2$O)$_4$(ox)$_4$(CH$_3$PO$_3$)]·2H$_2$O *Ln*=Nd, Pr) [23] and [Gd$_2$(ox)$_{2.5}${HO$_3$PCH$_2$NHCH$_2$(CH$_2$CH$_2$OPO$_2$)}(H$_2$O)$_2$]·5H$_2$O [24].

In this paper, we describe five new lanthanide compounds combining both 2-pyridylmethylphosphonate [(2-C$_5$H$_4$N)CH$_2$PO$_3$H$_2$, 2-pmpH$_2$] and oxalate ligands. Compounds [Ln_4(ox)$_5$(2-pmpH)$_2$(H$_2$O)$_7$]·5H$_2$O [*Ln*=Gd (**1**), Tb (**2**), Dy (**3**)] show a double layer structure, while compounds [Ln_4(ox)$_5$(2-pmpH)$_2$(H$_2$O)$_6$]·6H$_2$O [*Ln*=Ho (**4**), Yb (**5**)] exhibit a three-dimenisonal open framework structure.

2. Experimental section

2.1. Materials and methods

The 2-pyridylmethylphosphonic acid was prepared by a modified literature method [25]. All the other starting materials were of reagent quality and were obtained from commercial sources without further purification. Elemental analyses were performed on a Perkin Elmer 240C elemental analyzer. IR spectra were obtained as KBr disks on a VECTOR 22 spectrometer. Thermal analyses were performed in nitrogen in the temperature range 20–700 °C with a heating rate of 10 °C/min on a TGA-DTA V101B TA Inst 2100. The powder XRD patterns were recorded on a Shimadzu XD-3A X-ray diffractometer. The luminescent spectra were measured at room temperature on an Edinburg FL-FS920 fluorescence spectrometer. The magnetic susceptibility data of **1** were obtained on a polycrystalline sample, using a Quantum Design MPMS-XL7 SQUID magnetometer. Diamagnetic

* Corresponding author. Fax: +86 25 83314502.
E-mail addresses: lmzheng@nju.edu.cn, lmzheng@netra.nju.edu.cn (L.-M. Zheng).

0022-4596/$ - see front matter © 2010 Elsevier Inc. All rights reserved.
doi:10.1016/j.jssc.2010.03.008

corrections were made for both the sample holder and the compound estimated from Pascal's constants [26].

2.2. Syntheses of compounds **1–5**

Compounds **1–5** were obtained under the same experimental conditions. In a general synthesis, a mixture of $Ln(NO_3)_3 \cdot 6H_2O$ (0.05 mmol), 2-pmpH$_2$ (0.05 mmol) and $Na_2C_2O_4$(0.075 mmol) in 8 mL H_2O, was kept in a Teflon-lined autoclave at 160 °C for 5 d. Then the reaction system was slowly cooled to room temperature, and the corresponding colorless block-like crystals were obtained as a single phase, judged by the powder X-ray diffraction measurement. For **1**: Yield 54% based on Gd. Anal. Calcd. for $C_{22}H_{38}N_2O_{38}P_2Gd_4$: C, 16.22; H, 2.35; N, 1.72. Found: C, 16.27; H, 2.32; N, 1.59%. IR (KBr, cm^{-1}): 3374(br),1687(s), 1647(s), 1530(w), 1472(w), 1400(w), 1356(w), 1319(m), 1253(w), 1202(m), 1150(m), 1109(m), 1083(m), 1017(m), 920(w), 796(m), 752(w), 643(w), 605(w), 542(w), 484(w).

For **2**: Yield 49% based on Tb. Anal. Calcd. for $C_{22}H_{38}N_2O_{38}P_2Tb_4$: C, 16.15; H, 2.34; N, 1.71. Found: C, 16.17; H, 2.37; N, 1.71%. IR (KBr, cm^{-1}): 3378(br), 1687(s), 1647(s), 1529(w), 1472(w), 1425(w), 1400(w), 1356(w), 1319(m), 1253(w), 1201(m), 1150(m), 1110(m), 1084(m), 1016(m), 920(w), 878(w), 796(m), 752(w), 646(w), 605(w), 543(w), 483(w).

For **3**: Yield 44% based on Dy. Anal. Calcd. for $C_{22}H_{38}N_2O_{38}P_2Dy_4$: C, 16.01; H, 2.32; N, 1.70. Found: C, 16.01; H, 2.37; N, 1.71%. IR (KBr, cm^{-1}): 3379(br),1687(s), 1647(s), 1530(w), 1471(w), 1401(w), 1356(w), 1319(m), 1253(w), 1201(m), 1151(m), 1110(m), 1084(m), 1017(m), 920(w), 878(w), 796(m), 753(w), 643(w), 605(w), 542(w), 484(w).

For **4**: Yield 67% based on Ho. Anal. Calcd. for $C_{22}H_{38}N_2O_{38}P_2Ho_4$: C, 15.92; H, 2.31; N, 1.69. Found: C, 15.97; H, 2.27; N, 1.69%. IR (KBr, cm^{-1}): 3420(br), 3170(w), 3127(w), 1705(w), 1648(s), 1532(w), 1463(w), 1365(w), 1319(m), 1195(w), 1139(m), 1110(m), 1034(m), 923(w), 799(m), 759(w), 715(w), 637(w), 614(w), 549(w), 490(w).

For **5**: Yield 68% based on Yb. Anal. Calcd. for $C_{22}H_{38}N_2O_{38}P_2Yb_4$: C, 15.61; H, 2.26; N, 1.66. Found: C, 15.67; H, 2.21; N, 1.67. IR (KBr, cm^{-1}): 3402(br), 3170(w), 3126(w), 1709(w), 1653(s), 1532(w), 1463(w), 1365(w), 1321(m), 1120(w), 1145(m), 1115(m), 1039(m), 1004(w), 923(w), 800(m), 761(w), 721(w), 649(w), 614(w), 549(w), 488(w).

Thermal analyses reveal that each compound experiences the first step decomposition in the temperature range 30–250 °C, with the weight loss of 13.3% (calcd. 13.3%) for **1**, 13.6% (calcd. 13.2%) for **2**, 13.3% (calcd. 13.1%) for **3**, 12.5% (calcd. 13.0%) for **4**, and 12.3% (calcd. 12.8%) for **5**, corresponding to the release of 12 water molecules.

Table 2
Selected bond lengths (Å) for compounds **1**–**3**.

	1	2	3
Ln(1)–O(1)	2.287(5)	2.267(6)	2.253(6)
Ln(1)–O(4W)	2.374(5)	2.364(5)	2.363(6)
Ln(1)–O(7)	2.384(5)	2.373(5)	2.366(6)
Ln(1)–O(5W)	2.404(5)	2.382(5)	2.376(5)
Ln(1)–O(3W)	2.408(6)	2.389(6)	2.373(7)
Ln(1)–O(11)	2.415(5)	2.390(6)	2.384(6)
Ln(1)–O(8)	2.429(6)	2.437(5)	2.415(5)
Ln(1)–O(12)	2.439(5)	2.429(6)	2.416(6)
Ln(2)–O(2A)	2.216(5)	2.205(6)	2.194(6)
Ln(2)–O(15)	2.377(5)	2.375(5)	2.372(5)
Ln(2)–O(16)	2.390(5)	2.377(5)	2.367(6)
Ln(2)–O(2W)	2.390(5)	2.395(6)	2.374(6)
Ln(2)–O(25B)	2.406(5)	2.384(5)	2.369(6)
Ln(2)–O(14)	2.417(5)	2.403(6)	2.398(5)
Ln(2)–O(13)	2.437(6)	2.428(6)	2.415(6)
Ln(2)–O(26B)	2.444(5)	2.424(5)	2.418(6)
Ln(3)–O(4)	2.227(5)	2.215(5)	2.192(5)
Ln(3)–O(18)	2.386(5)	2.391(6)	2.380(5)
Ln(3)–O(17)	2.394(5)	2.393(5)	2.387(6)
Ln(3)–O(23)	2.397(5)	2.390(5)	2.378(6)
Ln(3)–O(1W)	2.415(5)	2.392(5)	2.384(6)
Ln(3)–O(19)	2.429(5)	2.401(5)	2.389(5)
Ln(3)–O(24)	2.446(5)	2.431(5)	2.419(6)
Ln(3)–O(20)	2.452(5)	2.440(6)	2.443(6)
Ln(4)–O(5)	2.240(6)	2.245(5)	2.231(5)
Ln(4)–O(6C)	2.275(5)	2.265(5)	2.246(6)
Ln(4)–O(21D)	2.443(5)	2.418(6)	2.408(6)
Ln(4)–O(22D)	2.445(5)	2.421(6)	2.417(6)
Ln(4)–O(9E)	2.451(5)	2.434(6)	2.431(6)
Ln(4)–O(10E)	2.453(5)	2.449(5)	2.448(6)
Ln(4)–O(6W)	2.481(5)	2.470(6)	2.456(5)
Ln(4)–O(7W)	2.534(5)	2.528(5)	2.512(6)

Symmetry codes: A: $x, y+1, z$; B: $x+1, y, z$; C: $-x, -y, -z+1$; D: $-x, -y+1, -z+1$; E: $-x+1, -y, -z+1$.

Table 1
Crystallographic data for compounds **1**–**5**.

Compound	1	2	3	4	5
Empirical formula	$C_{88}H_{152}N_8O_{152}P_8Gd_{16}$	$C_{88}H_{152}N_8O_{152}P_8Tb_{16}$	$C_{88}H_{152}N_8O_{152}P_8Dy_{16}$	$C_{11}H_{19}NO_{19}PHo_2$	$C_{11}H_{19}NO_{19}PYb_2$
Fw	6517.94	6544.66	6601.94	830.10	846.32
Crystal system	Monoclinic	Monoclinic	Monoclinic	Triclinic	Triclinic
Space group	$P2_1/c$	$P2_1/c$	$P2_1/c$	$P\bar{1}$	$P\bar{1}$
a (Å)	11.498(2)	11.4607(6)	11.4253(6)	9.7800(18)	9.6967(6)
b (Å)	10.564(2)	10.5623(5)	10.5386(6)	10.5058(18)	10.4415(7)
c (Å)	36.382(7)	36.3048(18)	36.209(2)	11.1899(19)	11.1027(7)
α (deg)	90	90	90	95.450(18)	95.090(3)
β (deg)	93.012(4)	93.1260(10)	93.2348(8)	92.327(12)	92.821(4)
γ (deg)	90	90	90	107.404(9)	107.231(3)
V (Å^3)	4413.1(15)	4388.2(4)	4352.9(4)	1089.2(3)	1066.07(12)
Z	1	1	1	2	2
D_c (g cm^{-3})	2.453	2.477	2.518	2.531	2.637
F(0 0 0)	3096	3112	3128	786	798
GOF on F^2	0.962	1.061	1.038	1.002	1.001
R_1, wR_2[a] [$I > 2\sigma(I)$]	0.0437, 0.0946	0.0402, 0.0859	0.0406, 0.0801	0.0377, 0.0773	0.0319, 0.0736
R_1, wR_2[a] (All data)	0.0626, 0.0987	0.0603, 0.0934	0.0644, 0.0882	0.0550, 0.0860	0.0435, 0.0840
$(\Delta\rho)_{max}$, $(\Delta\rho)_{min}$ (e Å^{-3})	0.701, −0.982	1.412, −1.827	1.600, −1.801	1.256, −1.295	1.256, −0.991

[a] $R_1 = \Sigma||F_o| - |F_c||/\Sigma|F_o|$. w$R_2 = [\Sigma w(F_o^2 - F_c^2)^2/\Sigma w(F_o^2)^2]^{1/2}$.

2.3. X-ray crystallographic analyses

Single crystals of dimensions $0.20\times0.18\times0.16\,mm^3$ for **1**, $0.28\times0.20\times0.16\,mm^3$ for **2**, $0.20\times0.18\times0.16\,mm^3$ for **3**, $0.12\times0.06\times0.04\,mm^3$ for **4** and $0.16\times0.12\times0.10\,mm^3$ for **5** were selected for indexing and intensity data collection at 298 K on a Bruker SMART APEX CCD diffractometer equipped with graphite-monochromatized MoKα ($\lambda=0.71073$ Å) radiation. A hemisphere of data was collected in the θ range 1.77–26.00° for **1**, 2.01–26.00° for **2**, 1.79–26.00° for **3**, 1.83–25.50° for **4** and 1.85–25.00° for **5** using a narrow-frame method with scan widths of 0.30° in ω and an exposure time of 10 s per frame. Numbers of measured and observed reflections [$I>2\sigma(I)$] are 22573 and 8564 ($R_{int}=0.0340$) for **1**, 23374 and 8559 ($R_{int}=0.0543$) for **2**, 23194 and 8514 ($R_{int}=0.0590$) for **3**, 5740 and 3980 ($R_{int}=0.0264$) for **4** and 5365 and 3668 ($R_{int}=0.0222$) for **5**, respectively. The data were integrated using the Siemens SAINT program [27], with the intensities corrected for Lorentz factor, polarization, air absorption, and absorption due to variation in the path length through the detector faceplate. Empirical absorption corrections were applied. The structures were solved by direct method and refined on F^2 by full matrix least-squares using SHELXTL [28]. All the non-hydrogen atoms were refined anisotropically. All H atoms were refined isotropically. Crystallographic and refinement details are listed in Table 1. Selected bond lengths and angles are given in Tables 2 and 3.

Table 3
Selected bond lengths (Å) for compounds **4** and **5**.

	4	5
Ln(1)–O(3A)	2.219(6)	2.180(6)
Ln(1)–O(1)	2.252(5)	2.225(6)
Ln(1)–O(5)	2.352(6)	2.333(6)
Ln(1)–O(4)	2.391(6)	2.361(6)
Ln(1)–O(8)	2.408(5)	2.375(6)
Ln(1)–O(9B)	2.414(6)	2.385(6)
Ln(1)–O(1W)	2.461(6)	2.418(6)
Ln(1)–O(2W)	2.463(6)	2.451(5)
Ln(2)–O(2)	2.158(6)	2.151(5)
Ln(2)–O(7C)	2.349(6)	2.330(6)
Ln(2)–O(13D)	2.357(5)	2.325(6)
Ln(2)–O(12)	2.366(5)	2.326(6)
Ln(2)–O(11E)	2.371(5)	2.326(5)
Ln(2)–O(10)	2.376(5)	2.333(6)
Ln(2)–O(3W)	2.417(6)	2.380(6)
Ln(2)–O(6C)	2.470(6)	2.453(6)

Symmetry codes: A: $-x$, $-y+1$, $-z$; B: $-x+1$, $-y+1$, $-z$; C: x, $y+1$, z; D: $-x+1$, $-y+2$, $-z+1$; E: $-x+1$, $-y+2$, $-z$.

3. Results and discussion

3.1. Description of structures 1–3

Compounds **1**–**3** are isostructural, and crystallize in the monoclinic space group $P2_1/c$. Hence only the structure of **1** will be discussed in detail as a representative. The building unit of **1** consists of four unique Gd atoms, two 2-pmpH$^-$ ligands, five oxalate anions, seven coordinated and five lattice water molecules. As shown in Fig. 1, four Gd atoms are each eight-coordinated. Around the Gd(1) atom, four positions are occupied by oxygen atoms [O(7), O(8), O(11), O(12)] from a pair of oxalate anions, and the remaining four sites are filled with a phosphonate oxygen [O(1)] from 2-pmpH$^-$ and three water molecules [O(3W), O(4W), O(5W)]. The Gd(2) and Gd(3) atoms are each surrounded by six oxalate oxygen atoms [O(13), O(14), O(15), O(16), O(25B), O(26B) for Gd(2) and O(17), O(18), O(19), O(22), O(23), O(24) for Gd(3)], one phosphonate oxygen [O(2A) for Gd(2) and O(4) for Gd(3)] and one water molecule [O(2W) for Gd(2) and O(1W) for Gd(3)]. The coordination sphere of Gd(4) is completed by four oxalate oxygen atoms [O(9E), O(10E), O(21D), O(22E)], two phosphonate oxygens [O(5), O(6C)], and two water molecules [O(6W), O(7W)]. The Gd–O bond distances and O–Gd–O bond angles are in the range of 2.216(5)−2.534(5) Å and 66.35(17)−153.82(17)°, respectively, comparable to those in compound

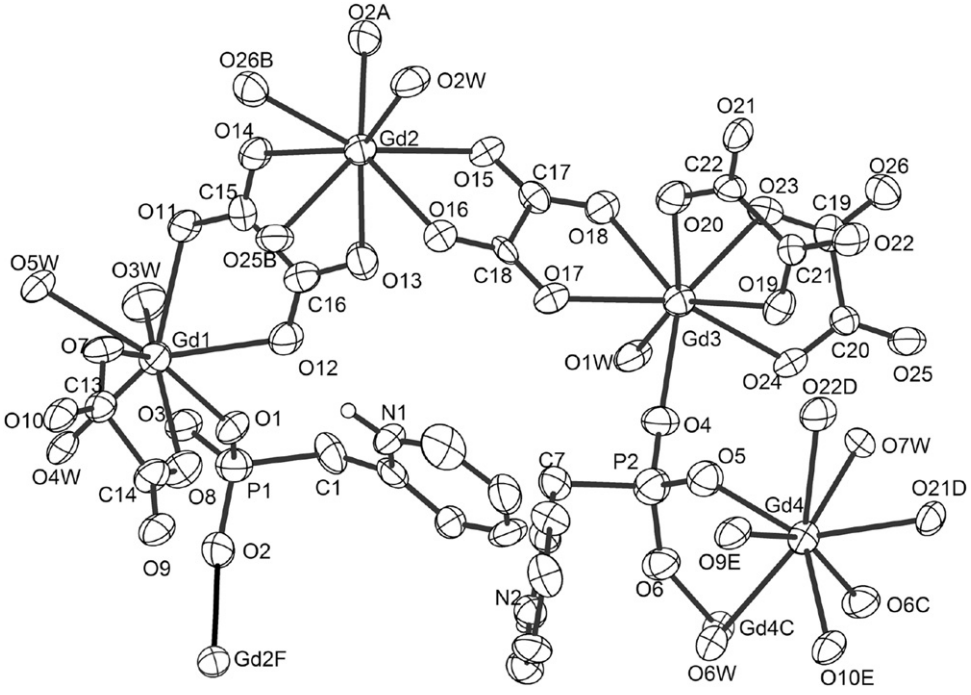

Fig. 1. Building unit of **1** with the labeling scheme (50% probability). All H atoms except those attached to the N atoms are omitted for clarity. Symmetry codes are the same as those given in Table 2.

$Gd(ox)\{MeNH(CH_2CO_2)(CH_2PO_3H)\}]\cdot 0.5H_2O$ [2.302(4)–2.486(4) Å,66.57(2)–158.65(2)°] [21].

Each oxalate anion serves as a tetra-dentate ligand, chelating and bridging the Gd atoms into a net-like layer of $\{Ln_4(ox)_5\}_n$ containing 40-membered rings of $Ln_{10}(ox)_{10}$ (Fig. 2, top). Two crystallographically distinguished 2-pmpH$^-$ ligands are found in the structure, showing a bi-dentate (P1-pmpH) and tri-dentate (P2-pmpH) coordination modes, respectively (Scheme 1). The P1-pmpH bridges Gd(1) and Gd(2F) atoms within the $\{Ln_4(ox)_5\}_n$ layer through two of its three phosphonate oxygens [O(1), O(2)]. The remaining phosphonate oxygen O(3) is pendent, and is involved in the hydrogen bond network. The P2-pmpH bridges Gd(3) and Gd(4C) within the $\{Ln_4(ox)_5\}_n$ layer, and also coordinates to the equivalent Gd(4) atom in the neighboring $\{Ln_4(ox)_5\}_n$ layer through O(5) atom. Consequently, a double layer is constructed (Fig. 2, bottom). The pyridyl groups of P1-pmpH reside on the two sides of the double layer, while those of P2-pmpH together with the lattice water molecules fill in the cavities within the double layer (Fig. 3). The double layers are further interconnected via hydrogen bonds among protonated pyridyl groups, uncoordinated phosphonate oxygens and water molecules, and forming a three dimensional supramolecular structure.

The structures of compounds **2** and **3** are analogous to **1** except that the Gd^{3+} ion in **1** is replaced by Tb^{3+} in **2**, and Dy^{3+} in **3**. The cell volumes decrease from **1** to **3**, in accordance with the decreasing sequence of the ionic radii of the corresponding metal ions.

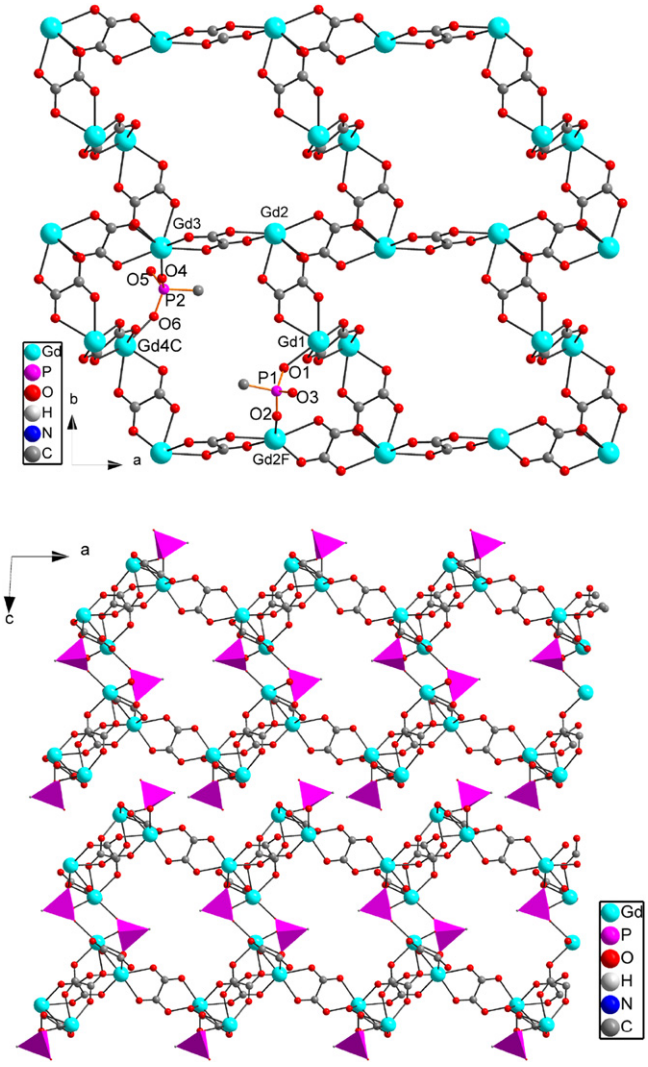

Fig. 2. Top: One layer of $\{Gd_4(ox)_5\}_n$ in compound **1**. Bottom: Double layer of structure **1**. Pyridyl groups and water molecules are omitted for clarity.

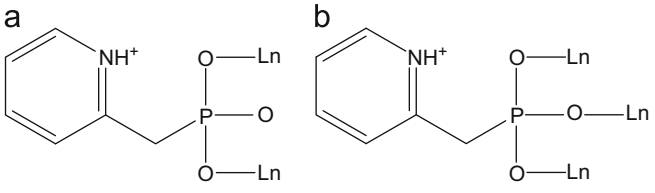

Scheme 1

3.2. Description of structures **4** and **5**

Compounds **4** and **5** are also isostructural, and crystallize in the triclinic space group $P-1$. Thus compound **4** is selected as an example. The asymmetric unit of **4** contains two unique Ho atoms, one 2-pmpH$^-$ ligand, two and a half unique oxalate anions, three coordinated and three lattice water molecules. As shown in Fig. 4, both Ho(1) and Ho(2) atoms are eight-coordinated. The eight positions around Ho(1) are occupied by four oxygen atoms [O(4), O(5), O(8), O(9B)] from two oxalate anions, two phosphonate oxygens [O(1), O(3A)] from two equivalent 2-pmpH$^-$ ligands, and two water molecules [O(1W), O(2W)]. The Ho(2) atom is surrounded by six oxygen atoms [O(6C), O(7C), O(10), O(11E), O(12), O(13D)] from three oxalate anions, one phosphonate oxygen O(2) from the 2-pmpH$^-$ ligand and a water molecule O(3W). The Ho–O bond lengths fall in the range 2.219(6)–2.470(6) Å, which are comparable to those in $Ho_2Cu_3(C_5H_4NPO_3)_6$ [29].

A $\{Ho_4(ox)_5\}_n$ layer containing $Ho_{10}(ox)_{10}$ rings is also observed in **4**, similar to those in **1–3**. However, each 2-pmpH$^-$ in **4** behaves as a tri-dentate ligand, bridging Ho(1) and Ho(2) atoms within the $\{Ho_4(ox)_5\}_n$ layer and between the layers through its three phosphonate oxygen atoms. Thus a three dimensional open framework is formed, which can be described as $\{Ho_4(ox)_5\}_n$ layers cross-linked via corner-sharing $\{HoO_8\}$ and $\{PO_3C\}$ polyhedra. The generated cavities are filled with protonated pyridyl groups and lattice water molecules (Fig. 5).

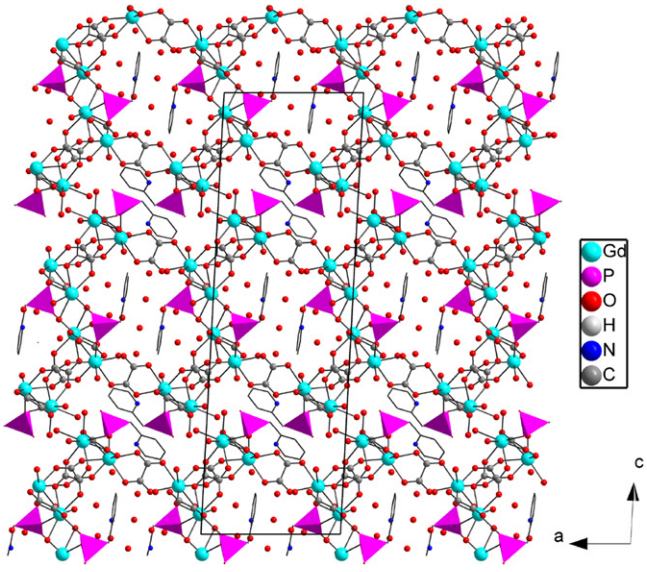

Fig. 3. Structure **1** viewed down the *b*-axis.

Structure **5** is identical to **4** except that the Ho^{3+} ion is replaced by Yb^{3+} in **5**. The cell volume of **5** is decreased comparing with that of **4**.

It is noted that compounds **1–5** were synthesized under similar conditions. Although all have the same molecular composition, two types of structures are found depending on different lanthanide ions. Compounds **1–3** show double layer structures, separated by the bi-dentate $pmpH^-$ ligands. While in compounds **4** and **5**, all $pmpH^-$ serve as tri-dentate ligands and link the *Ln*–ox layers into a three dimensional open framework. Such structural difference could be attributed to the effect of lanthanide contraction. Similar phenomenon has been observed in a few other lanthanide phosphonate systems [18,30].

3.3. Luminescent and magnetic properties

The solid-state luminescent properties of compounds **1–3** were investigated at room temperature. Compound **1** exhibits a broad blue fluorescent emission band at $\lambda_{max}=448$ nm ($\lambda_{ex}=340$ nm) (Fig. 6), which corresponds to a ligand-centered (LC) fluorescence. The metal-centered (MC) electronic levels of Gd^{3+} ion are known to be located at 31,000 cm^{-1}, well above the ligand-centered electronic levels of organic ligands. Therefore, ligand-to-metal energy transfer and the consequent MC luminescence cannot be observed [31]. Under excitation of 370 nm, compound **2** emits strong green luminescence characteristic for the Tb^{3+} ions, with four emission bands at about 480, 545, 584 and 621 nm corresponding to $^5D_4 \rightarrow {}^7F_J$ ($J=6, 5, 4, 3$) transitions (Fig. 7, top) [32,33]. Excitation of

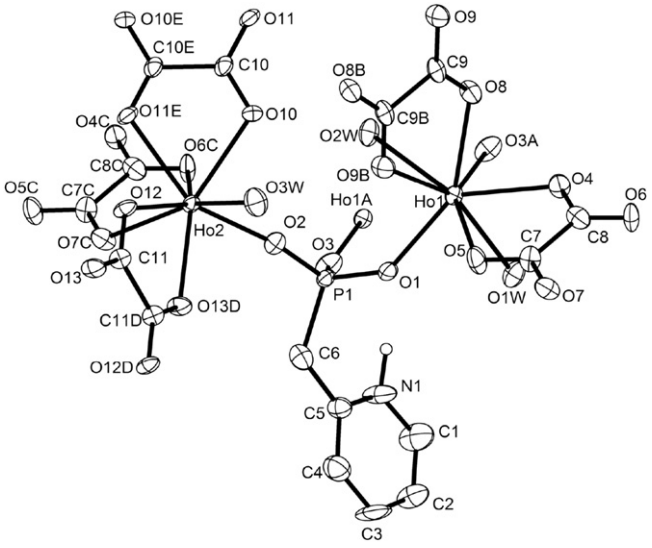

Fig. 4. Building unit of **4** with the labeling scheme (50% probability). All H atoms except that attached to N1 were omitted for clarity. Symmetry codes are the same as those given in Table 3.

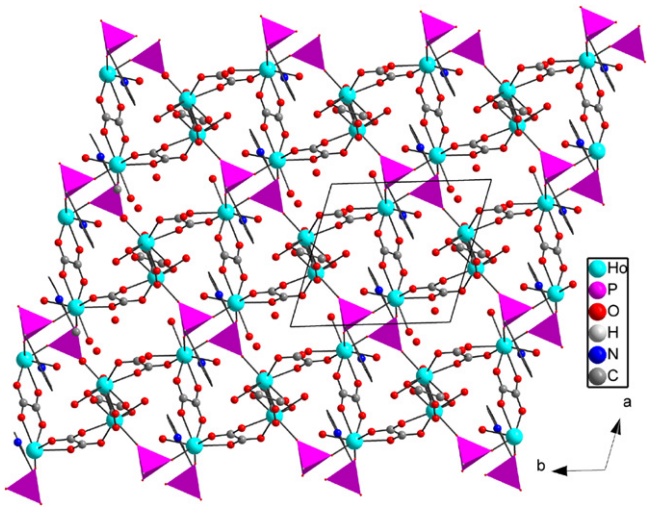

Fig. 5. Structure **4** viewed down the *c*-axis.

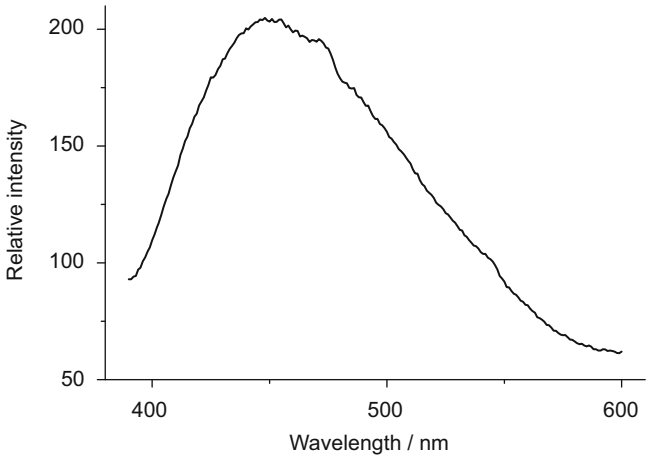

Fig. 6. Emission spectrum of **1** in solid state.

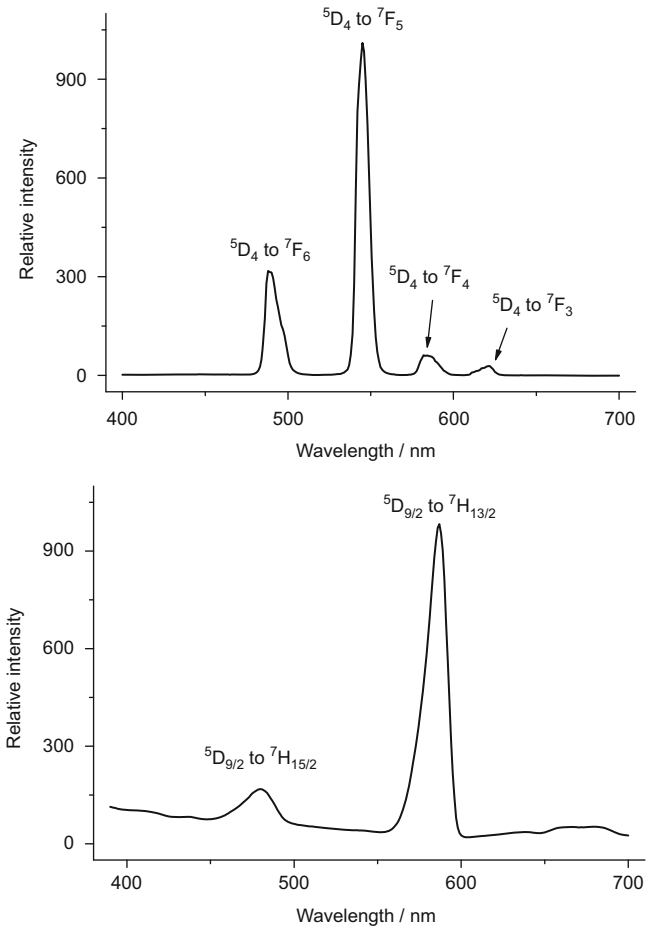

Fig. 7. Emission spectra of **2** (top) and **3** (bottom) in solid state.

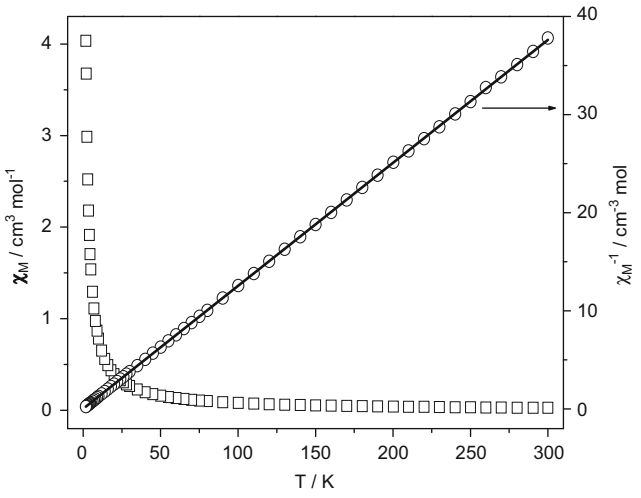

Fig. 8. The χ_M and $\chi_M{}^{-1}$ versus T plots for compound **1**.

complex **3** at 285 nm leads to a yellow luminescent emission typical for Dy^{3+}. The two bands at 480 and 587 nm are attributed to transitions of $^4D_{9/2}\rightarrow{}^6H_{15/2}$ and $^4D_{9/2}\rightarrow{}^6H_{13/2}$, respectively (Fig. 7, bottom). The decay for **2** and **3** could be best fit by a biexponential process. The corresponding lifetimes are $\tau_1=784.56\,\mu s$ (99.58%) and $\tau_2=21.74\,\mu s$ (0.42%) for **2**, and $\tau_1=0.92\,\mu s$ (84%) and $\tau_2=5.41\,\mu s$ (16%) for **3**, comparable to other corresponding Ln^{3+} complexes [34,35].

Fig. 8 shows the χ_M and χ_M^{-1} versus T plots for compound **1**. At 300 K, the effective magnetic moment per Gd (7.97 μ_B) is very close to the spin only value of 7.94 μ_B for $S=7/2$. The magnetic behavior of **1** follows the Curie–Weiss law in the whole temperature range with a Curie constant of 7.98 $cm^3\,K\,mol^{-1}$ and a Weiss constant $\theta=-0.149$ K. The small value of Weiss constant suggests that the magnetic coupling between Gd(III) ions is very weak, thus the magnetic behavior of **1** is paramagnetic.

4. Conclusions

Five new lanthanide oxalatophosphonates $[Ln_4(ox)_5(2\text{-pmpH})_2(H_2O)_7]\cdot 5H_2O$ [Ln^{3+}=Gd (**1**), Tb (**2**), Dy (**3**)] and $[Ln_4(ox)_5(2\text{-pmpH})_2(H_2O)_6]\cdot 6H_2O$ [Ln(III)=Ho (**4**), Yb (**5**)] are obtained by using 2-pyridylmethylphosphonic acid (2-$pmpH_2$) in the presence of oxalate anion. In all cases, $\{Ln_4(ox)_5\}_n$ layers containing $Ln_{10}(ox)_{10}$ rings are found, which are linked by phosphonate groups of 2-$pmpH^-$ into a double layer in the cases of **1–3**, and 3D open framework in the cases of **4** and **5**. More interestingly, compounds **1–3** show blue, green and yellow luminescent emissions, respectively. The results demonstrate that luminescent lanthanide phosphonates with new architectures may be obtained through the introduction of a second bridging ligand. Further work is in progress to synthesize mixed ligated metal phosphonates with interesting optical and magnetic properties.

Acknowledgments

This work is supported by NSFC (no. 90922006), the National Basic Research Program of China (2007CB925102 and 2010CB923402), NSF of Jiangsu Province (no. BK2009009) and NSFC for Creative Research Group (no. 20721002).

Appendix A. Supplementary Material

Supplementary data associated with this article can be found in the online version at doi:10.1016/j.jssc.2010.03.008.

References

[1] A. Clearfield, Prog. Inorg. Chem. 47 (1998) 371.
[2] G. Ferey, Chem. Soc. Rev. 37 (2008) 191.
[3] A. Clearfield, Dalton Trans. (2008) 6089.
[4] M.-A. Haga, K. Kobayashi, K. Terada, Coord. Chem. Rev. 251 (2007) 2688.
[5] R. Vivani, G. Alberti, F. Costantino, M. Nocchetti, Microporous Mesoporous Mater. 107 (2008) 58.
[6] A. Hu, G.T. Yee, W. Lin, J. Am. Chem. Soc. 127 (2005) 12486.
[7] S.-S. Bao, L.-F. Ma, Y. Wang, L. Fang, C.-J. Zhu, Y.-Z. Li, L.-M. Zheng, Chem. Eur. J. 13 (2007) 2333.
[8] A.V. Palii, O.S. Reu, S.M. Ostrovsky, S.I. Klokishner, B.S. Tsukerblat, Z.-M. Sun, J.-G. Mao, A.V. Prosvirin, H.-H. Zhao, K.R. Dunbar, J. Am. Chem. Soc. 130 (2008) 14729.
[9] S. Khanra, M. Kloth, H. Mansaray, C.A. Muryn, F. Tuna, E.C. Sanudo, M. Helliwell, E.J.L. McInnes, R.E.P. Winpenny, Angew. Chem. Int. Ed. 46 (2007) 5568.
[10] D. Cave, F.C. Coomer, E. Molinos, H.-H. Klauss, P.T. Wood, Angew. Chem. Int. Ed. 45 (2006) 803.
[11] Y.-S. Ma, Y.-Z. Li, Y. Song, L.-M. Zheng, Inorg. Chem. 47 (2008) 4536.
[12] X.-G. Liu, S.-S. Bao, Y.-Z. Li, L.-M. Zheng, Inorg. Chem. 47 (2008) 5525.
[13] M. Carraro, A. Sartorel, G. Scorrano, C. Maccato, M.H. Dickman, U. Kortz, M. Bonchio, Angew. Chem. Int. Ed. 47 (2008) 7275.
[14] H.C. Aspinall, Chem. Rev. 102 (2002) 1807.
[15] J.-C.G. Bünzli, C. Piguet, Chem. Soc. Rev. 34 (2005) 1048.
[16] J. Xia, B. Zhao, H.-S. Wang, W. Shi, Y. Ma, H.-B. Song, P. Cheng, D.-Z. Liao, S.-P. Yan, Inorg. Chem. 46 (2007) 3450.
[17] X.-P. Yang, R.A. Jones, J. Am. Chem. Soc. 127 (2005) 7686.
[18] J.-G. Mao, Coord. Chem. Rev. 251 (2007) 1493.
[19] C.N.R. Rao, S. Natarajan, R. Vaidhyanathan, Angew. Chem. Int. Ed. 43 (2004) 1466.
[20] L.Z. Zhang, W. Gu, B. Li, X. Liu, D.Z. Liao, Inorg. Chem. 46 (2007) 622.
[21] J.-L. Song, J.-G. Mao, Chem. Eur. J. 11 (2005) 1417.
[22] S.-M. Ying, J.-G. Mao, Crystal Growth Des. 6 (2006) 964.
[23] Y.-L. Huang, M.-Y. Huang, T.-H. Chan, B.-C. Chang, K.-H. Lii, Chem. Mater. 19 (2007) 3232.
[24] Y. Zhao, J. Li, Z.-G. Sun, J. Zhang, Y.-Y. Zhu, X. Lu, L. Liu, N. Zhang, Inorg. Chem. Commun. 11 (2008) 1057.
[25] X.-M. Gan, I. Binyamin, B.M. Rapko, J. Fox, E.N. Duesler, R.T. Paine, Inorg. Chem. 43 (2003) 2443.
[26] O. Kahn, Molecular Magnetism, VCH Publishers, Inc., New York, 1993.
[27] SAINT, Program for Data Extraction and Reduction, Siemens Analytical X-ray Instruments, Madison, WI, 1994–1996.
[28] SHELXTL (version 5.0), Reference Manual, Siemens Industrial Automation, Analytical Instruments, Madison, WI, 1995.
[29] Y.-S. Ma, H. Li, J.-J. Wang, S.-S. Bao, R. Cao, Y.-Z. Li, J. Ma, L.-M. Zheng, Chem. Eur. J. 13 (2007) 4759.
[30] B. Liu, B.-L. Li, Y.-Z. Li, Y. Chen, L.-M. Zheng, Inorg. Chem. 46 (2007) 8524.
[31] W.-K. Wong, H. Liang, J. Guo, W.-Y. Wong, W.-K. Lo, K.-F. Li, K.-W. Cheah, Z. Zhou, W.-T. Wong, Eur. J. Inorg. Chem. (2004) 829.
[32] S.-F. Tang, J.-L. Song, X.-L. Li, J.-G. Mao, Cryst. Growth Des. 6 (2006) 2322.
[33] J. Rohovec, P. Vojtisek, P. Hermann, J. Mosinger, Z. Zak, I. Lukes, J. Chem. Soc. Dalton Trans. (1999) 3585.
[34] Y.G. Huang, B.L. Wu, D.Q. Yuan, Y.Q. Xu, F.L. Jiang, M.C. Hong, Inorg. Chem. 46 (2007) 3450.
[35] S. Comby, R. Scopelliti, D. Lmbert, L. Charbonniere, R. Ziessel, J.G. Bunzli, Inorg. Chem. 45 (2006) 3158.